Cai et al discuss the enhancement of secondary organic aerosol downwind of urban centers due to increased partitioning of semi-volatile vapors. FIGAERO-CIMS is employed to assess the volatility evolution of particulate species over time. PMF is applied to SP-AMS data in order to understand the sources of OA. Overall the work is thorough and the limitations are clearly stated. I think the content of the work is appropriate for ACP and therefore I would recommend publication after the following comments are addressed.

1. I greatly appreciate the transparency of the PMF factors being provided in the SI, however, more description of these factors and how they were determined is required in the main text. Each factor should be described individually and it should be discussed why it was attributed to the specific source it was. Particularly, the Night-OA, BBOA, and aBBOA factors seem visually quite similar and a discussion of the specific difference would be very helpful. Additionally the average composition values for HOA and aBBOA are identical which seems surprising.

Reply: We appreciate the reviewer for this valuable suggestion. The composition values for HOA are copy mistake and has been revised. A comment from reviewer 3 states that the lower O:C and higher H:C of aBBOA factor is contrary to what it is expected for aging. Our results indicate that this factor was likely formed through oxidation of biomass burning precursors rather the aging process of BBOA. To avoid any confusion, we renamed this factor as biomass burning SOA (BBSOA). Additionally, we have modified section 2.2.2 by providing more description of these factors.

"The PM_1 chemical composition was measured by a soot particle aerosol mass spectrometer (SP-AMS, Aerodyne Research, Inc., USA). The details of the operation and data analysis can be found in Kuang et al. (2021). Source apportionment was performed for organic aerosols in the bulk PM_1 using positive matrix factorization (PMF). The organic aerosol could be divided into six components, including two primary OA factors and four secondary OA factors. The mass spectral profiles of six OA factors are shown in Figure S3. The timeseries and diurnal variation of these factors are presented in Figure S4.

The primary OA factors include hydrocarbon-like OA (HOA), mainly contributed by traffic and cooking emissions and biomass burning OA (BBOA) originating from biomass burning combustion. The HOA was identified by hydrocarbon ions $C_xH_y^+$. Owing to the prominent hydrocarbon ions and low O:C value (0.10), HOA could be attributed to primary emission from cooking and traffic. The BBOA was recognized by the markers $C_2H_4O_2^+$ (m/z 60.022, 0.5%) and $C_3H_5O_2^+$ (m/z 73.029, 0.4%), which are considered tracers for biomass burning OA (Ng et al., 2011).

The SOA factors include biomass burning SOA (BBSOA) likely formed from oxidation of biomass burning emission, less oxygenated OA (LOOA) provided by strong daytime photochemical formation, more oxygenated OA (MOOA) related to regional transport, and nighttime-formed OA (Night-OA) contributed by secondary formation during nighttime. The BBSOA was likely formed through oxidation of biomass burning precursors, which was supported by the evening peak at about 19:00 LT (Fig. S4). BBSOA showed a similar variation trend with $C_6H_2NO_4^+$, which might be contributed by oxidation of gaseous precursors from biomass burning emissions (Wang et al., 2019; Bertrand et al., 2018). The significant afternoon peak of LOOA indicates its formation through photochemical reactions, which would be detailly discussed in

section 3.1. The negligible diurnal variation and the highest O:C value (1.0) of MOOA suggested that it could be aged OA resulting from long-range transport. Night-OA was formed through NO_3 nighttime chemistry, supported by a pronounced evening elevation and positive correlation with nitrate (R=0.67).The detailed determination of PMF factors has been found in Kuang et al. (2021) and Luo et al. (2022).

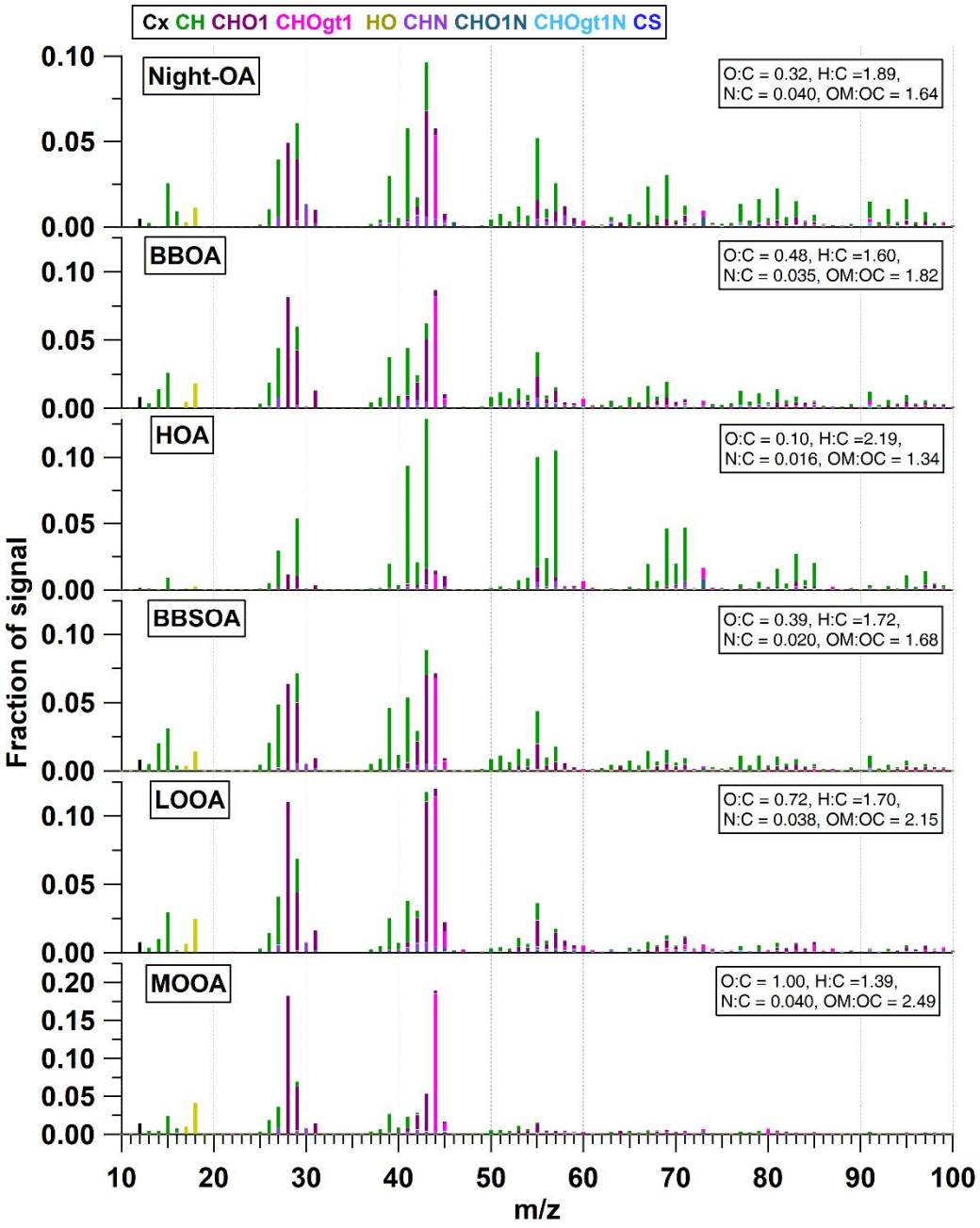

Figure S3. Mass spectral profile of six OA factors. The colors represent different family groups.

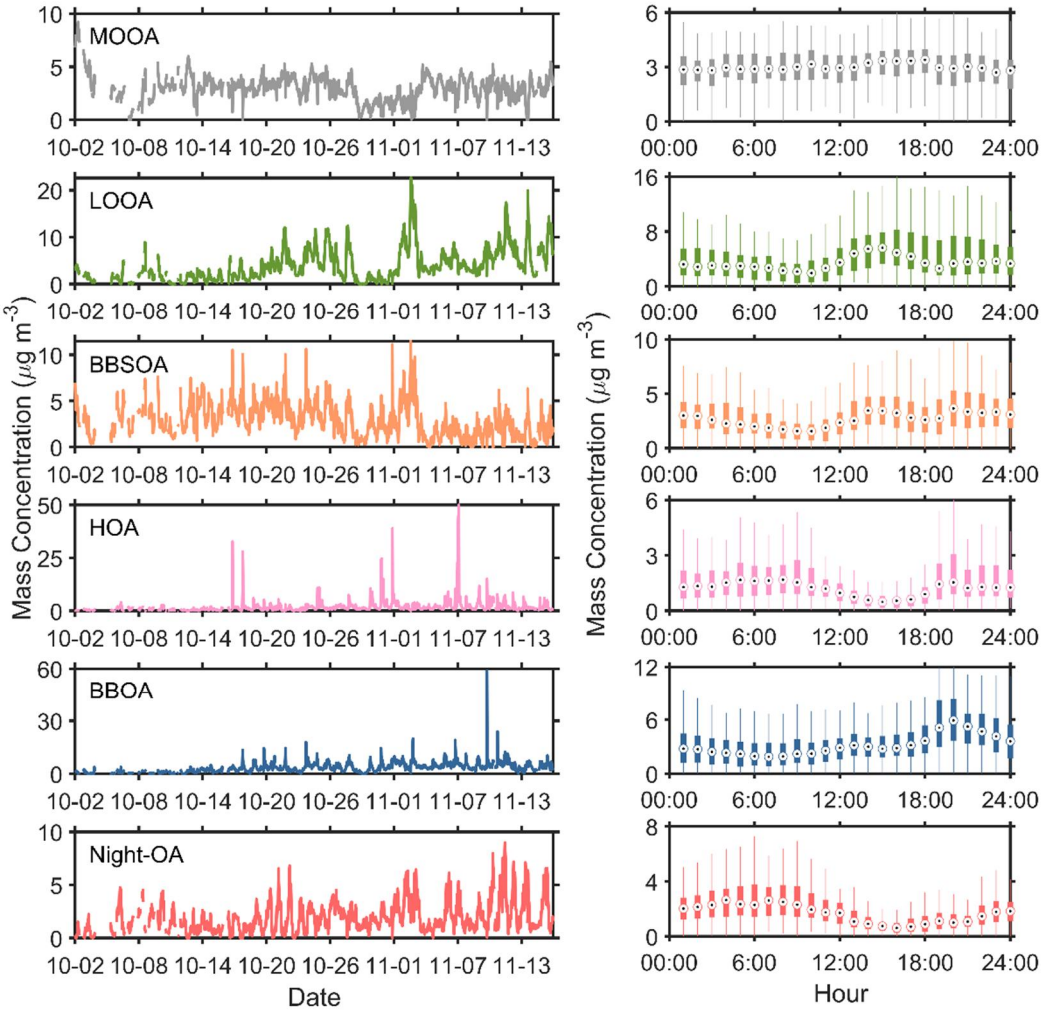

Figure S4. Timeseries and diurnal variation of six OA factors.

”

2. This is likely beyond the scope of this study, but I wonder if any consideration was given to using PMF to identify different sources or formation pathways from the FIGAERO-CIMS data as in Buchholz et al as well as other studies. Perhaps just an idea for future work.

Reply: We are grateful to the reviewer for this valuable suggestion. Buchholz et al. (2020) employed PMF to the FIGAERO-CIMS data in the laboratory study. However, performing PMF analysis to the campaign thermograms data is challenging, since the amount of data is huge. After a lot of effort, we have successfully conducted a PMF analysis of the campaign thermograms data. The 20s averaged data were input into the PMF model. The data processing method, such as error schemes, was based on Buchholz et al. (2020). An example of our results can be found in the following figure (fig. 2.1). We are still analyzing our results; we hope to publish them soon.

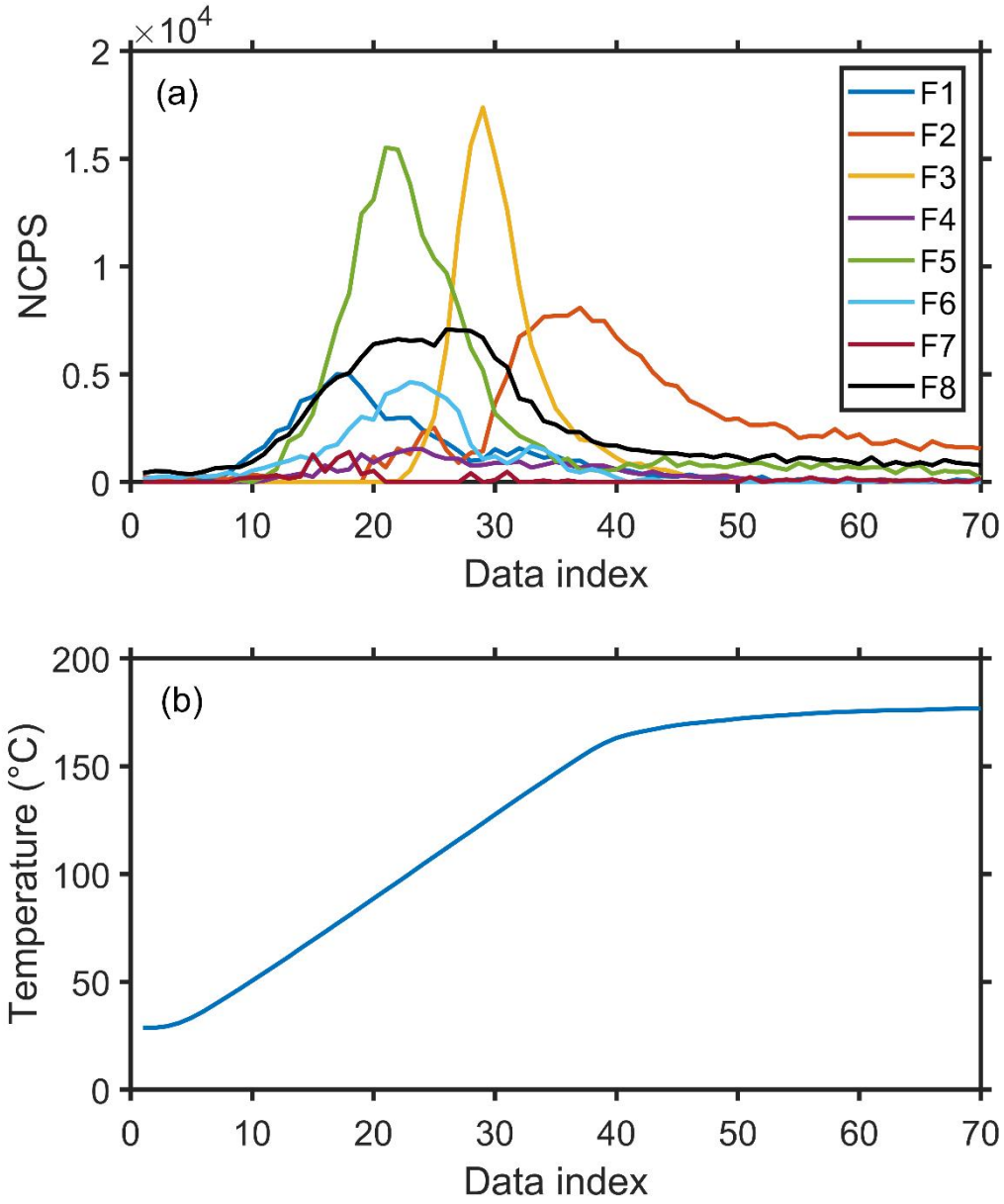

Figure 2.1. The (a) PMF thermogram factors and (b) desorption temperature against data point index.

3. Line 168: A MW of 200 g mol^{-1} is assumed, but can you not retrieve an average MW from the CIMS data? Would it be biased too high due to low detection efficiency of less oxidized, low MW species?

Reply: We appreciate the reviewer for this valuable suggestion. We calculated the average molecular weight based on the CIMS data. It shows that the average molecular weight of particle-phase compounds was 194.9 g mol^{-1}, which was close to the assumed M_w (200 g mol^{-1}). We noticed that using a universal M_w value in the C^* estimation of each compound could lead to a deviation. Ylisirniö et al. (2021) calculated the C^* based on the M_w of the compound determined

by the FIGAERO-CIMS, we believed it would be a better way in calculating the C^*. The comparison of the estimated C^* based on the universal M_w and actual M_w was shown in the following figure (Fig. 3.1). It suggested that adopting a universal M_w value (200 g mol^{-1}) could lead to an overestimate of C^* for compounds with a M_w lower than 200 g mol^{-1}, while this trend was overturned for species was a M_w higher than 200 g mol^{-1}.

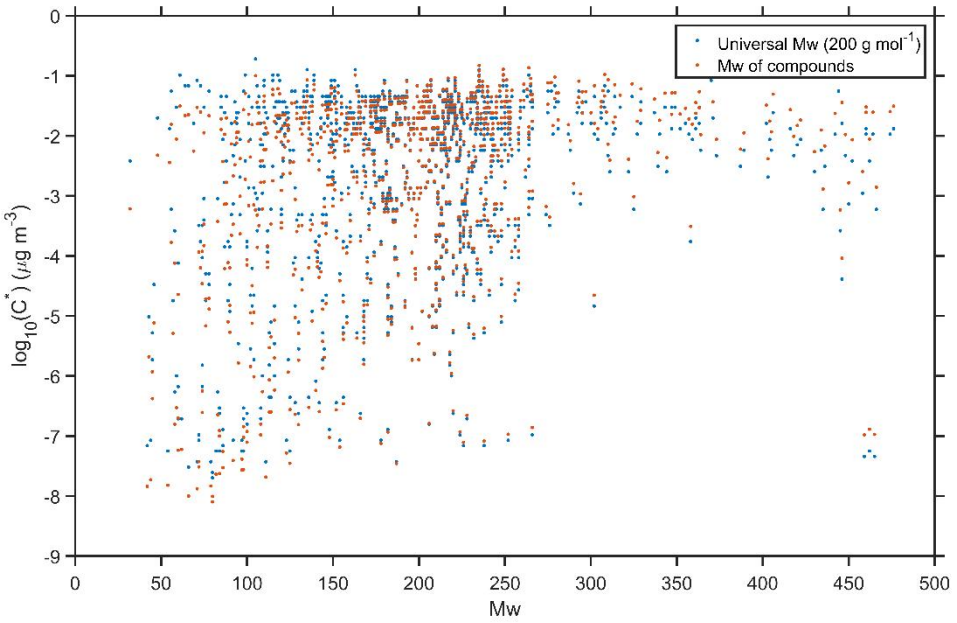

Figure 3.1. The estimated C^* based on the universal M_w and actual M_w.

Thus, we used the M_w of the compound in eq. (2) and modified the corresponding discussion and figures in our manuscript.

Line 348-352, "Table 1 investigated the relationship between SVOC+LVOC and six OA factors. The SVOC+LVOC in FIGAERO OA had a significant positive correlation (R=0.72-0.85) with the LOOA, especially during the urban air masses period (R=0.85, Fig. S14 and Table 1), suggesting that the LOOA formation was mainly responsible for the increase of OA volatility.

Table 1. The correlation coefficient between SVOC+LVOC in FIGAERO OA and six OA factors in AMS OA during different periods.

	All campaign	Long-range Transport	Urban Air Masses	Coastal Air Masses
MOOA	-0.004	0.02	0.11	-0.19
LOOA	0.83	0.74	0.85	0.72
BBSOA	0.47	0.48	0.75	0.14
HOA	0.11	0.18	-0.11	0.61
BBOA	0.57	0.55	0.55	0.77
Night-OA	0.35	0.39	0.07	0.53

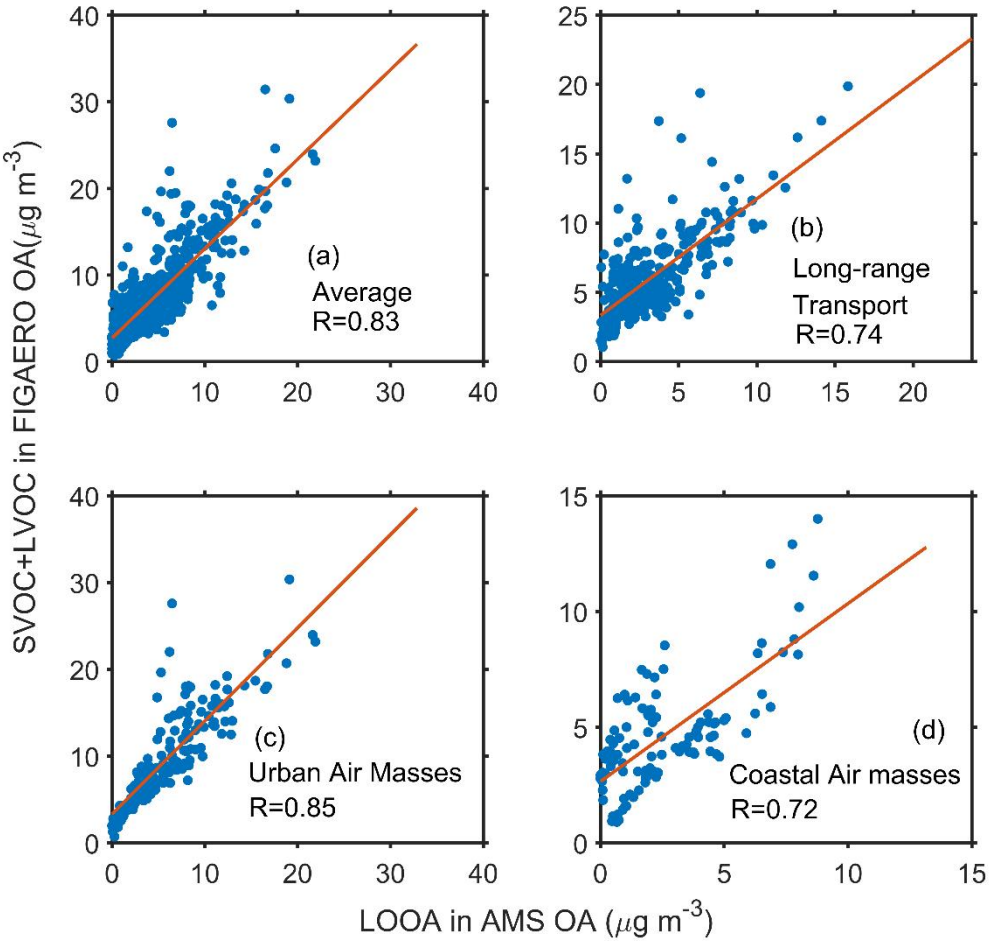

Figure S14. Relationship between the SVOC+LVOC in FIGAERO OA and LOOA in AMS OA during (a) the whole campaign, (b) long-range transport, (c) urban air masses, and (d) coastal air masses periods.

”

Figure 5,

“

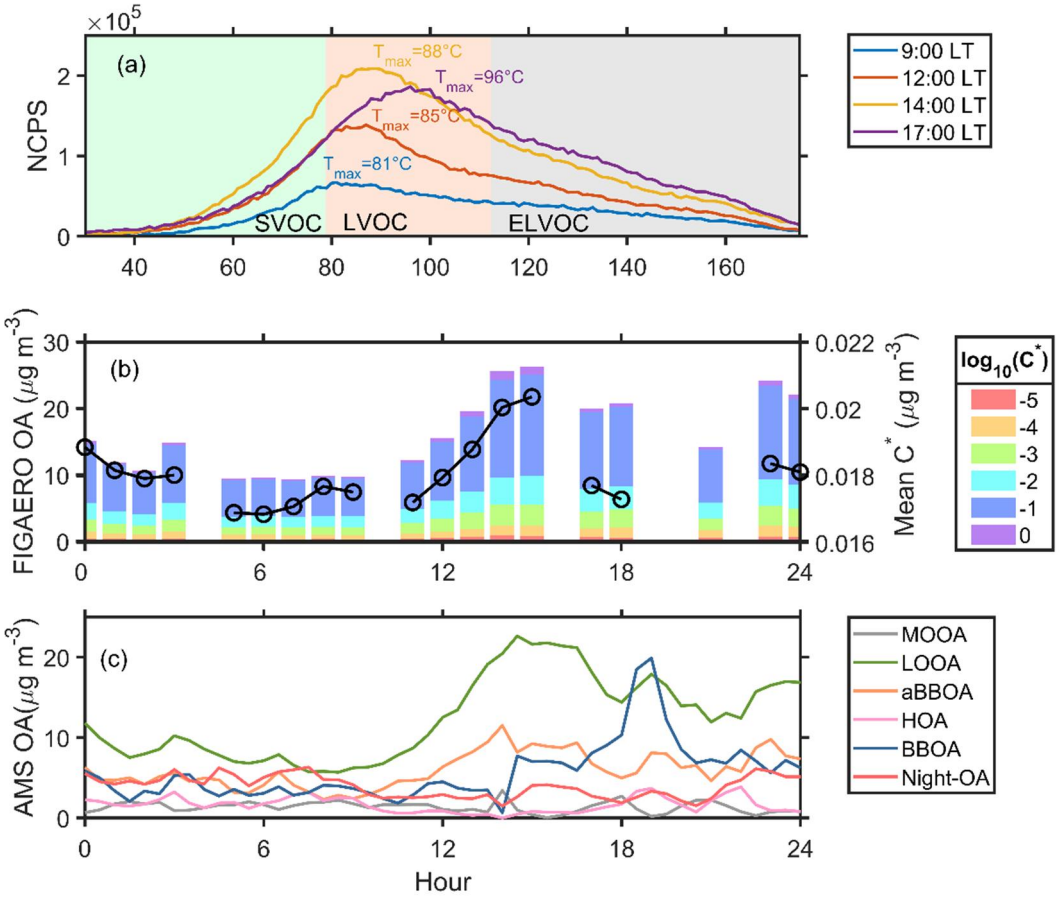

Figure 5. (a) The sum thermograms at 9:00, 12:00, 14:00, and 17:00, (b) variation of FIGAERO OA volatility presented in a volatility range from 10^{-5} to 10^{0} μg m^{-3} and mean C^*, and (c) variation of six OA factors from PMF analysis on 2 November 2019. The mean $C^*(\overline{C^*})$ is estimated as $\overline{C^*} = 10^{\sum f_i log_{10} C_i^*}$, where f_i is the mass fraction of OA with a volatility C_i^*.

”

4. The determination of the volatility of gas-phase species is based on the formation pathway of the species. This is important to consider due to the different functional groups likely to be dominant in products formed via autoxidation and I applaud the authors consideration of this. Given the uncertainties associated with the volatility estimation, the method employed in this study is likely good enough, however, as explicit determination of the pathway of formation is impossible, some discussion of this limitation should be added. I also think a sentence describing how H:C and O:C (Fig S6) were used to determine the pathway of formation as well as relevant references in the main text would be helpful.

Reply: We appreciate the reviewer for this valuable suggestion. We have modified the corresponding sentences by adding some discussion about the limitations and how to determine the pathway in the main text. Also, we have revised the slope of black line in the Van-Krevelen diagram, since the previous one was a copy mistake.

Line 214-218, “For gas-phase organic compounds (organic vapors), we first divided them into two groups based on their potential oxidation pathways (multi-generation OH oxidation and autoxidation, solid line in Fig. S7) and then used different parameters in their volatility estimation. The classification of pathways was based on the molecular characteristics of oxidation products of aromatics and monoterpene, respectively (Wang et al., 2020).

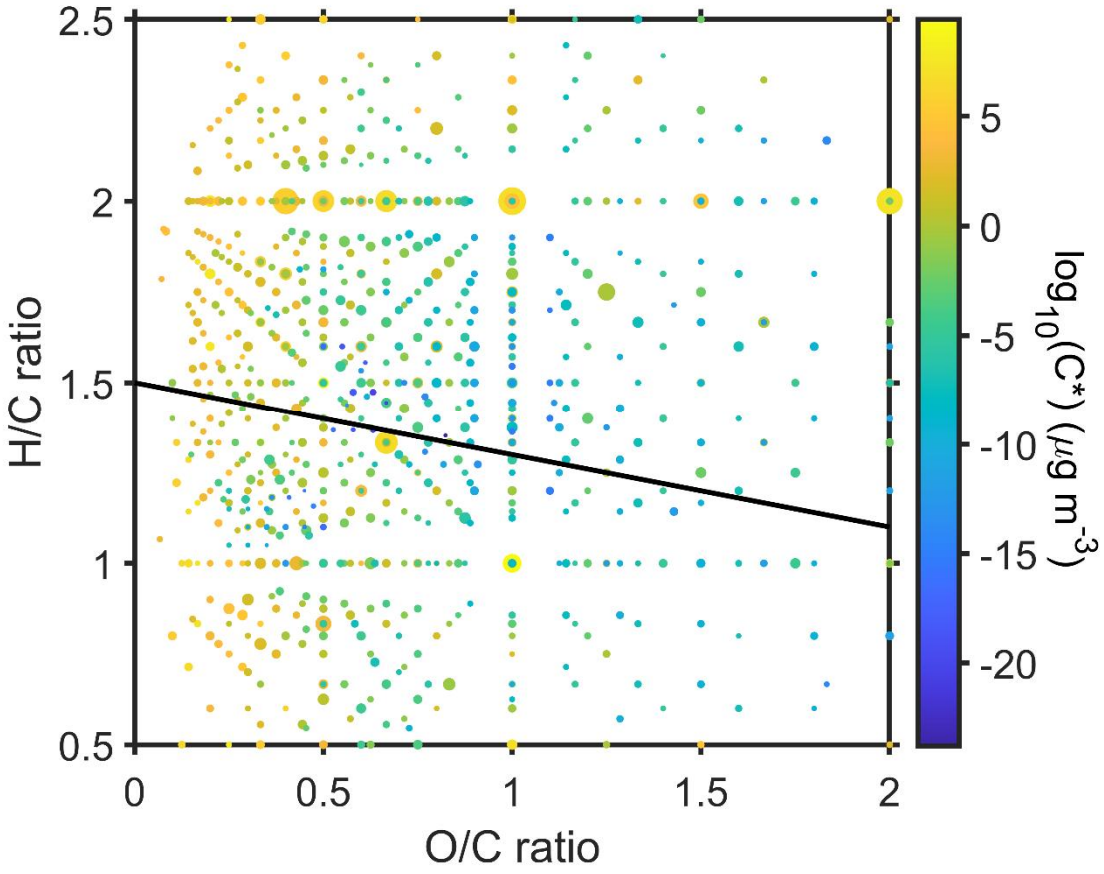

Figure S7. Van-Krevelen diagram (O/C ratio versus H/C ratio) of gas-phase organic compounds measured by FIGAERO-CIMS. The symbol size is proportional to the mass concentration of organic vapors and the color code represents the volatility. The black solid line divided the organic vapors potentially formed through the autoxidation pathway (upper regime) and multi-generation OH oxidation pathway (lower regime), based on the oxidation products aromatics and monoterpene, respectively (Wang et al., 2022; Wang et al., 2020).

”

Line 225-227, “It should be noted that this method can only roughly distinguish the formation pathways of ambient organic vapors, since it is based on the oxidation products of specific species in a laboratory study”.”

5. I am confused about the assignment of species with C*>$10^{0.5}$ as “non-condensable.” This boundary is within the SVOC VBS range and particularly under the high mass loadings one

could see even downwind of urban plumes, it seems species with higher volatilities may contribute substantially to the particle phase. Is this determination specific to the conditions of this study in some way or based on other literature?

Reply: We appreciate the reviewer for this valuable suggestion. Nie et al. (2022) calculated the contribution of condensing organic vapor to the formation of SOA. For organic vapor with relatively lower volatility (C^* ≤0.01 μg m^{-3}), the condensation to particle-phase was regarded as irreversible. Wang et al. (2022) integrated organic vapor from the lowest volatility bin to $C^* \leq 10^{0.5}$ μg m^{-3} and regard them as condensable vapors. Our assignment of organic vapors was based on Wang et al. (2022). We noticed that using the name "non-condensable organic vapors" and "condensable organic vapors" could lead to confusion, since "non-condensable organic vapors" can also reach the particle phase through gas-particle partitioning. Thus, we modified the classification, ELVOC and LVOC are classified as low volatility organic vapors ($C^* \leq 0.3$ μg m^{-3}), while SVOC, IVOC and VOC fall into another category regarded as high volatility organic vapors ($C^* > 0.3$ μg m^{-3}). The corresponding sentences and figures in the manuscript have been revised.

6. While stated correctly in the text, I think the boundary of the SVOC class is incorrect in Fig 4b. SVOCs should extend to $10^{-0.5}$ not $10^{0.5}$ ug m^{-3}, assuming these are C*(300 K).

Reply: We are grateful to the reviewer for this valuable suggestion. We have revised the boundary of the SVOC in fig. 3, fig. 4, and fig. S12.

"

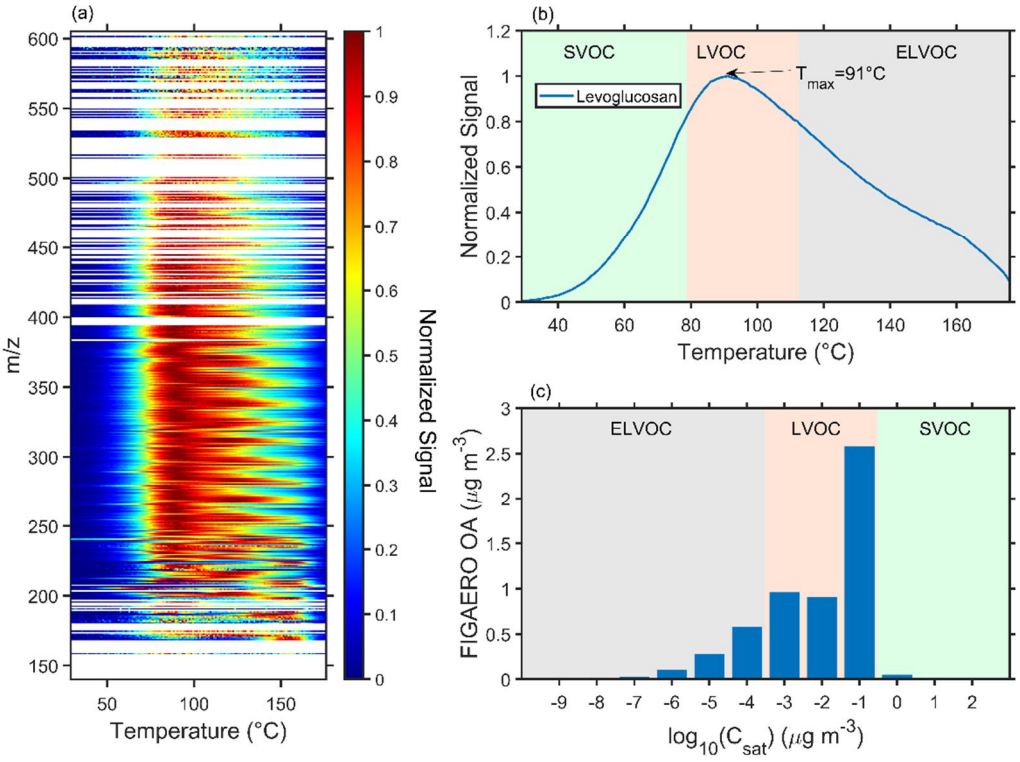

Figure 3. The average (a) two-dimensional thermograms of all calibrated and semi-quantified species, (b) one-dimensional thermogram of levoglucosan, and (c) volatility distribution of all calibration and semi-quantified species in the particle phase measured by the FIGAERO-CIMS (referred as FIGAERO OA). The T_{max} was converted to the C^* according to Eqs. (1) and (2).

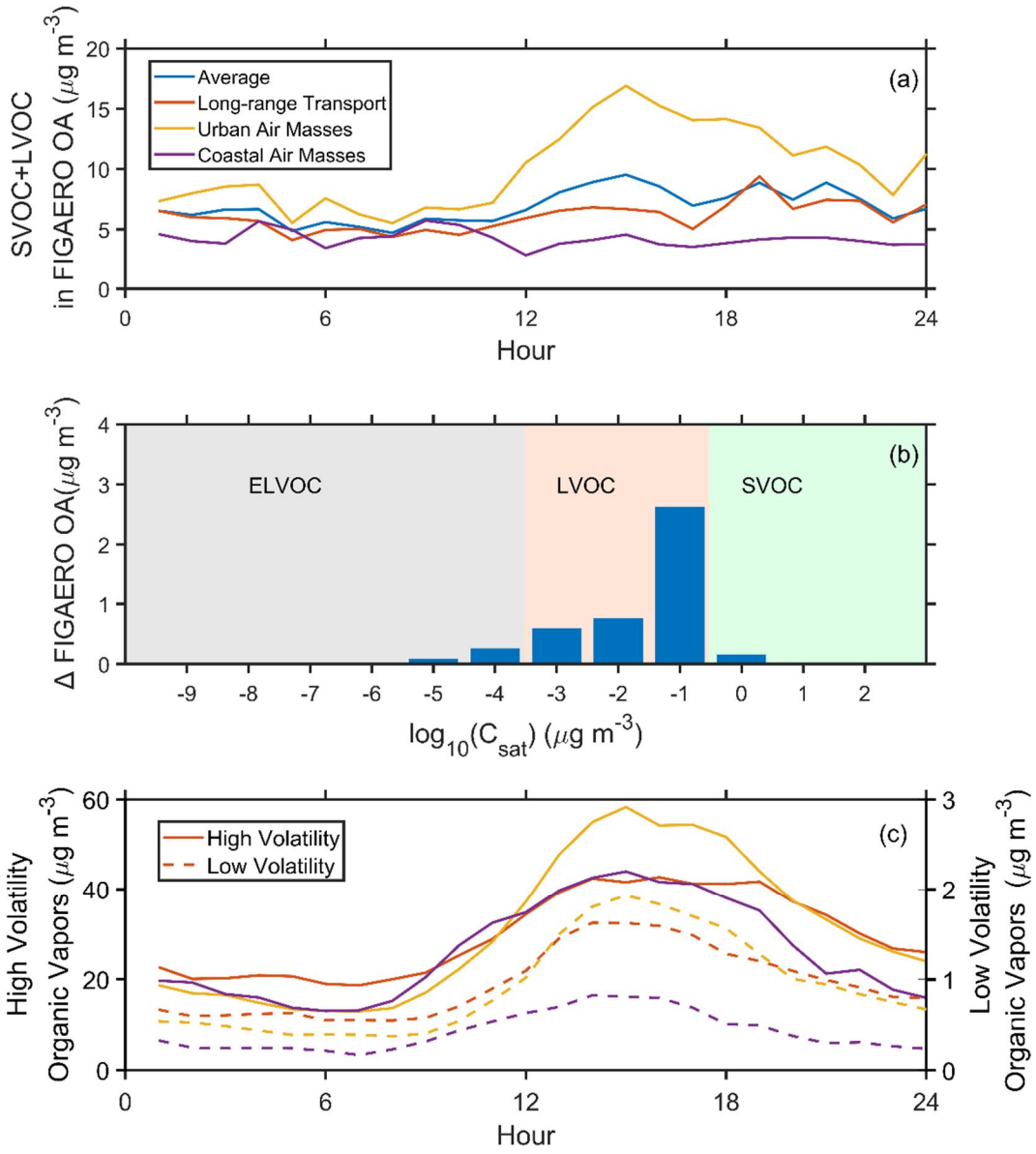

Figure 4. Diurnal variation of (a) SVOC+LVOC in FIGAERO OA, (b) the difference of FIGAERO OA between the urban air masses and long-range transport periods, and (c) low volatility organic vapors (ELVOC+LVOC, solid lines) and high volatility organic vapors (SVOC+IVOC+VOC, dash lines) during the whole campaign and three selected periods.

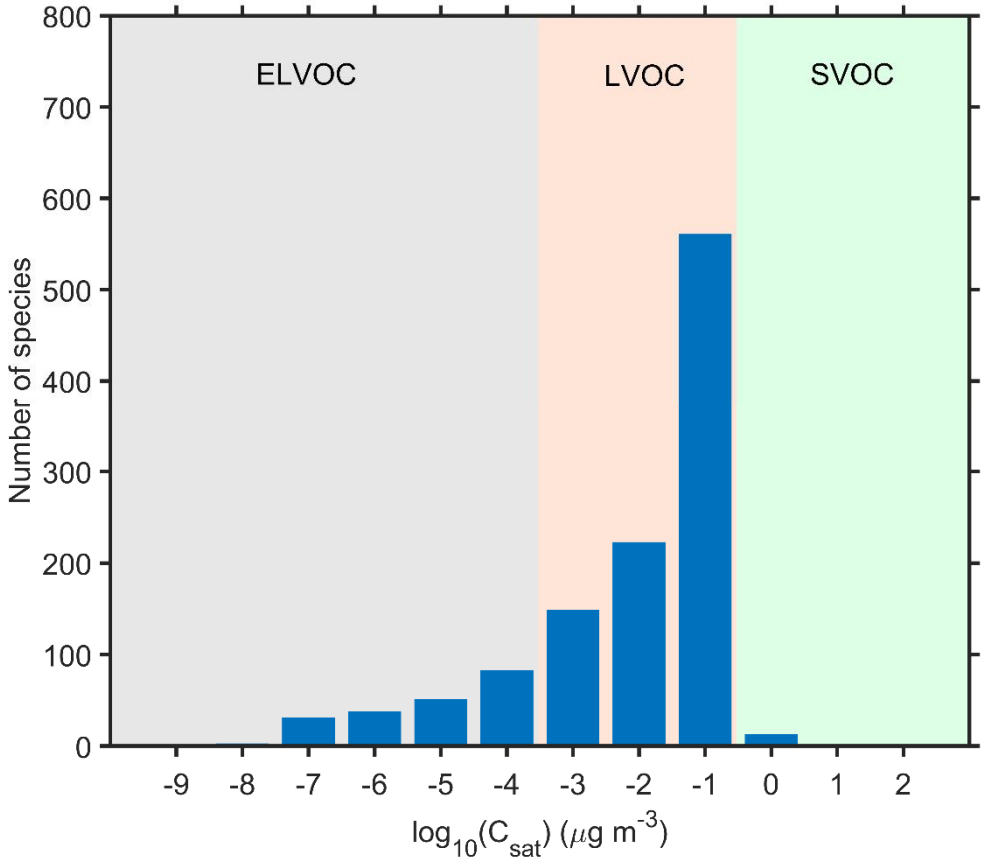

Figure S12. Volatility distribution of the number of calibrated and semi-quantified species measured by the FIGAERO-CIMS.

”

References

Bertrand, A., Stefenelli, G., Jen, C. N., Pieber, S. M., Bruns, E. A., Ni, H., Temime-Roussel, B., Slowik, J. G., Goldstein, A. H., El Haddad, I., Baltensperger, U., Prévôt, A. S. H., Wortham, H., and Marchand, N.: Evolution of the chemical fingerprint of biomass burning organic aerosol during aging, Atmos. Chem. Phys., 18, 7607-7624, 10.5194/acp-18-7607-2018, 2018.

Buchholz, A., Ylisirniö, A., Huang, W., Mohr, C., Canagaratna, M., Worsnop, D. R., Schobesberger, S., and Virtanen, A.: Deconvolution of FIGAERO–CIMS thermal desorption profiles using positive matrix factorisation to identify chemical and physical processes during particle evaporation, Atmos. Chem. Phys., 20, 7693-7716, 10.5194/acp-20-7693-2020, 2020.

Kuang, Y., Huang, S., Xue, B., Luo, B., Song, Q., Chen, W., Hu, W., Li, W., Zhao, P., Cai, M., Peng, Y., Qi, J., Li, T., Wang, S., Chen, D., Yue, D., Yuan, B., and Shao, M.: Contrasting effects of secondary organic aerosol formations on organic aerosol hygroscopicity, Atmos. Chem. Phys., 21, 10375-10391, 10.5194/acp-21-10375-2021, 2021.

Luo, B., Kuang, Y., Huang, S., Song, Q., Hu, W., Li, W., Peng, Y., Chen, D., Yue, D., Yuan, B., and Shao, M.: Parameterizations of size distribution and refractive index of biomass burning organic

aerosol with black carbon content, Atmos. Chem. Phys., 22, 12401-12415, 10.5194/acp-22-12401-2022, 2022.
Ng, N. L., Canagaratna, M. R., Jimenez, J. L., Zhang, Q., Ulbrich, I. M., and Worsnop, D. R.: Real-Time Methods for Estimating Organic Component Mass Concentrations from Aerosol Mass Spectrometer Data, Environmental Science & Technology, 45, 910-916, 10.1021/es102951k, 2011.
Nie, W., Yan, C., Huang, D. D., Wang, Z., Liu, Y., Qiao, X., Guo, Y., Tian, L., Zheng, P., Xu, Z., Li, Y., Xu, Z., Qi, X., Sun, P., Wang, J., Zheng, F., Li, X., Yin, R., Dallenbach, K. R., Bianchi, F., Petäjä, T., Zhang, Y., Wang, M., Schervish, M., Wang, S., Qiao, L., Wang, Q., Zhou, M., Wang, H., Yu, C., Yao, D., Guo, H., Ye, P., Lee, S., Li, Y. J., Liu, Y., Chi, X., Kerminen, V.-M., Ehn, M., Donahue, N. M., Wang, T., Huang, C., Kulmala, M., Worsnop, D., Jiang, J., and Ding, A.: Secondary organic aerosol formed by condensing anthropogenic vapours over China's megacities, Nature Geoscience, 10.1038/s41561-022-00922-5, 2022.
Wang, M., Chen, D., Xiao, M., Ye, Q., Stolzenburg, D., Hofbauer, V., Ye, P., Vogel, A. L., Mauldin, R. L., Amorim, A., Baccarini, A., Baumgartner, B., Brilke, S., Dada, L., Dias, A., Duplissy, J., Finkenzeller, H., Garmash, O., He, X.-C., Hoyle, C. R., Kim, C., Kvashnin, A., Lehtipalo, K., Fischer, L., Molteni, U., Petäjä, T., Pospisilova, V., Quéléver, L. L. J., Rissanen, M., Simon, M., Tauber, C., Tomé, A., Wagner, A. C., Weitz, L., Volkamer, R., Winkler, P. M., Kirkby, J., Worsnop, D. R., Kulmala, M., Baltensperger, U., Dommen, J., El-Haddad, I., and Donahue, N. M.: Photo-oxidation of Aromatic Hydrocarbons Produces Low-Volatility Organic Compounds, Environmental Science & Technology, 54, 7911-7921, 10.1021/acs.est.0c02100, 2020.
Wang, Y., Hu, M., Wang, Y., Zheng, J., Shang, D., Yang, Y., Liu, Y., Li, X., Tang, R., Zhu, W., Du, Z., Wu, Y., Guo, S., Wu, Z., Lou, S., Hallquist, M., and Yu, J. Z.: The formation of nitro-aromatic compounds under high NOx and anthropogenic VOC conditions in urban Beijing, China, Atmos. Chem. Phys., 19, 7649-7665, 10.5194/acp-19-7649-2019, 2019.
Wang, Y., Clusius, P., Yan, C., Dällenbach, K., Yin, R., Wang, M., He, X.-C., Chu, B., Lu, Y., Dada, L., Kangasluoma, J., Rantala, P., Deng, C., Lin, Z., Wang, W., Yao, L., Fan, X., Du, W., Cai, J., Heikkinen, L., Tham, Y. J., Zha, Q., Ling, Z., Junninen, H., Petäjä, T., Ge, M., Wang, Y., He, H., Worsnop, D. R., Kerminen, V.-M., Bianchi, F., Wang, L., Jiang, J., Liu, Y., Boy, M., Ehn, M., Donahue, N. M., and Kulmala, M.: Molecular Composition of Oxygenated Organic Molecules and Their Contributions to Organic Aerosol in Beijing, Environmental Science & Technology, 56, 770-778, 10.1021/acs.est.1c05191, 2022.
Ylisirniö, A., Barreira, L. M. F., Pullinen, I., Buchholz, A., Jayne, J., Krechmer, J. E., Worsnop, D. R., Virtanen, A., and Schobesberger, S.: On the calibration of FIGAERO-ToF-CIMS: importance and impact of calibrant delivery for the particle-phase calibration, Atmos. Meas. Tech., 14, 355-367, 10.5194/amt-14-355-2021, 2021.